Supporting Information

Zak et al. 10.1073/pnas.1107577108

SI Materials and Methods

qRT-PCR. Total RNA was isolated from bone marrow-derived macrophages using TRIzol (Invitrogen) and used as template for reverse transcription (Superscript II, Invitrogen) according to the manufacturer's instructions. *Il12b*, *Il8*, and *Nfkbia* transcript levels were measured using the Applied Biosystems Taqman assays Mm99999067_m1, Mm00434226_m1, and Mm00477798_m1, respectively, with Taqman Fast (Applied Biosystems) master mix. *Il1b* and *Il1a* transcript levels were measured using Fast SYBR Green master mix (Applied Biosystems) and the following primers (IDT): Il1a-F (5′-GTGTTGCTGAAGGAGTTGCCAGAA-3′), Il1a-R (5′-GTGCACCCGACTTTGTTCTTTGGT-3′), Il1b-F (5′-AAGAGCTTCAGGCAGGCAGTATCA-3′), and Il1b-R (5′-TAATGGGAACGTCACACACCAGCA-3′). Data were acquired on a 7900HT Fast Real-Time PCR system (Applied Biosystems) and were normalized to the expression of *Eef1a1* mRNA transcripts in individual samples measured by Taqman assays using the following primers (IDT): Eef1a1-F (5′-GCAAAAACGACCCACCAATG-3′), Eef1a1-R (5′-GGCCTGGATGGTTCAGGATA-3′), and Eef1a1-Probe (5′-FAM-CACCTGAGCAGTGAAGCCAG-3′-TAMRA). For all experiments, fold induction was computed with respect to the normalized expression levels of respective wild-type macrophages under unstimulated conditions within the same experiment. Tests for significant differences were performed by Bonferonni posttests of repeated measures two-way ANOVA (Graphpad PRISM).

Microarrays. Total RNA was isolated from bone marrow-derived macrophages using TRIzol (Invitrogen). Before labeling, the integrity of samples was checked using an Agilent 2100 Bioanalyzer.

Agilent arrays. RNA samples from $Sharpin^{cpdm}$, $Ikbkg^{panr2}$, $Atf3^{-/-}$, $Nfkb1^{-/-}$, $Il10^{-/-}$, and respective wild-type control macrophages were analyzed from two independent experiments using the Agilent SurePrint G3 Mouse GE 8 × 60K microarray platform. Labeling was performed with the One-Color Microarray-Based Gene Expression Analysis protocol version 6.5 (Agilent). Briefly, double-stranded cDNA was synthesized from 200 ng of total RNA using a T7-oligo(dT) primer, followed by in vitro transcription by T7 RNA polymerase with incorporation of Cy3-labeled CTP. A total of 600 ng of Cy3-labeled cRNA was hybridized in Agilent hybridization chambers for 17 h at 65 °C and at 10 rpm. The arrays were washed for 1 min in Agilent GE Wash Buffer 1 and then for another minute in Agilent GE Wash Buffer 2. Scanning was performed using an Agilent High-Resolution DNA Microarray Scanner with 3-μm resolution and 20-bit dynamic range. The resulting images were processed with Agilent Feature Extraction version 10.7.3.1 to generate raw probe intensity data. Arrays were normalized using the "normalize.quantiles" function in the Bioconductor (1) package *preprocessCore*. Repeated measurements for a given gene were averaged in the following manner: *1*) Simple averages were computed for repeated measurements of individual probes, and *2*) then weighted averages based on 90% expression quantiles were sequentially computed for repeated measures of RefSeq IDs, Entrez gene IDs, and gene symbols.

Affymetrix arrays. RNA samples from $Map3k8^{sluggish}$, $Tnf^{-/-}$, and respective wild-type control macrophages were analyzed from two independent experiments (except for $Tnf^{-/-}$, measured in singlet) using Affymetrix Mouse Exon ST 1.0 microarrays, which were prepared, hybridized, and scanned according to the manufacturer's instructions. Briefly, biotinylated cDNA was generated from 2 μg total RNA and hybridized onto microarrays for 16 h at 45 °C. The microarrays were washed and stained with streptavidin–phycoerythrin using an Affymetrix FS-450 fluidics station, and data were collected with the Affymetrix GeneChip Scanner 3000. Microarrays were normalized at the gene level using the BrainArray custom CDF (2) (Entrez Gene, Version 14) for probeset definitions and RMA (3) as implemented in the "justRMA" function of the Bioconductor (1) package *affy* for background adjustment, quantile normalization, and summarization. Normalized Agilent and Affymetrix microarray data were merged on the basis of Entrez Gene ID (when possible) or gene symbol.

Microarray Analysis. ***Gene set enrichment analysis.*** Genes induced at least threefold by Pam_3CSK_4 (300 ng/mL, 12 h) in two independent experiments in the relevant wild-type control macrophages for $Sharpin^{cpdm}$ (C57BL/KaLawRij) were first selected. The effects of SHANK-associated RH domain-interacting protein (SHARPIN) deficiency on the induction of these 400 genes was then determined by comparing poststimulation expression levels in homozygous $Sharpin^{cpdm}$ macrophages with expression levels in C57BL/KaLawRij macrophages from the same experiment. For genes with expression levels consistently impaired or enhanced in two independent experiments, the effect of SHARPIN deficiency was conservatively taken as the value from the replicate with the smallest absolute effect. For genes not consistently impaired or enhanced between the two experiments, the effect of SHARPIN deficiency was taken to be zero. Genes were then ordered by the magnitude of SHARPIN effects, with the most impaired at the top and the most enhanced at the bottom (Fig. 2*A*). Transcription factor (TF) binding site predictions for the complete set of 400 Pam_3CSK_4-induced genes were obtained using PAINT (4), which automatically retrieves promoter sequences and scans them for the presence of TRANSFAC (5) TF-binding matrices. TRANSFAC public binding site predictions meeting a core similarity threshold of 0.9 were obtained for promoters 500 and 2,000 bp from the transcription start site. To address the redundancy of TRANSFAC matrix definitions, we merged the binding predictions for matrices according to the matrix clusters defined in ref. 6. TF matrix clusters not detected in the promoters of at least 4 genes or detected in more than 200 genes were excluded from subsequent analysis. The TF-binding predictions were then merged with the effects of SHARPIN deficiency, defined above using the Gene Set Enrichment Analysis (GSEA) framework as described in ref. 7. The statistical significance (*P* values) of the computed GSEA enrichment scores for the TF matrix clusters was estimated by performing 100,000 gene-based permutations of the dataset. False discovery rates (FDR) were computed from the enrichment *P* values using the Benjamini–Hochberg method (8). The only two TF matrix clusters significantly associated with the effects of SHARPIN deficiency on Pam_3CSK_4 were #5 (compiled NF-κB sites) in 500-bp promoters and #20 (compiled AP-1 sites) in 2,000-bp promoters. The scaled heat-map visualization of the results (Fig. 2*A*) was generated using Treeview (9).

Interaction network analysis. The putative NF-κB interaction network was constructed by appending the list of Pam_3CSK_4-induced genes defined above with the NF-κB TFs RELA and REL and then by using InnateDB (10) to retrieve the known interactions between all 402 genes. The overall network was pruned to contain only the genes regulated by NF-κB TFs (RELA, REL, NFKB1, NFKBIZ), as defined by protein–DNA interactions, and the NF-κB TFs themselves. The resulting network was imported into Cytoscape (11) and nodes were colored according to the effects of SHARPIN deficiency as defined

above. The putative AP-1 interaction network was constructed similarly, but by using the AP-1 TFs (FOS, JUN, JUNB, JUND, ATF2, BATF, and BATF3) in place of the NF-κB TFs.

Comparative expression analysis. Genes induced at least twofold by Pam_3CSK_4 (300 ng/mL, 12 h) in two independent experiments in the relevant wild-type control macrophages for all mutants (*Sharpin*^{cpdm}, *Ikbkg*^{panr2}, *Nfkb1*$^{-/-}$, *Atf3*$^{-/-}$, *Map3k8*^{sluggish}, *Il10*$^{-/-}$, and *Tnf*$^{-/-}$) were first selected. The effects of the various mutations on the induction of these 251 genes were then determined by comparing poststimulation expression levels in mutant macrophages with expression levels in control macrophages from the same experiment. For genes with expression levels consistently impaired or enhanced by a given mutation in two independent experiments, the effects of the mutation were conservatively taken as the value from the replicate with the smallest absolute effect. For genes not consistently impaired or enhanced between the two experiments, the effect of the mutation was taken to be zero. The effects of the *Tnf*$^{-/-}$ mutation were defined by comparing the single set of array data with two sets of wild-type controls. The effects of the mutations were assembled into a matrix and clustered using the Self Organizing Maps module in Cluster (9) and visualized using Treeview (9).

Expression Constructs and Cloning. Expression constructs for epitope-tagged human SHARPIN, RBCK1, and *N*F-κB *E*ssential *Mo*dulator (NEMO) were generated by cloning cDNA amplified from pOTB7-hSHARPIN, pDNR-Lib-hSHARPIN, and pENTR223-hIKBKG (all Open Biosystems) into the expression vectors pBEN2F, pBEC2H [FLAG- and HA-tag–expressing derivatives of pEF6 (12)], and pEF-DEST51 (Invitrogen). The NEMO L153P point mutation was generated by site-directed mutagenesis using the primers F_hNEMO_L153P (gtgacgtccttgctcggggagc-P) and R_hNEMO_L153P (aagcgactctggctctcctgGG). All construct integrities were confirmed by sequencing.

Immunoprecipitation and Immunoblotting. For immunoprecipitation (IP), HEK293 cells were transfected with the respective constructs using Lipofectamine 2000 (Invitrogen). Thirty-six hours later, cells were lysed for 20 min with IP buffer [20 mM Hepes (pH 7.4), 110 mM KOAc, 2 mM $MgCl_2$, 150 mM NaCl, 0.5% Triton X-100, 0.1% Tween-20, and proteinase inhibitor and phosphatase inhibitor mixtures (both Roche)] on ice and spun to remove insoluble components and nuclei. IP was performed with 8 μL M2 anti-FLAG magnetic beads (Sigma Aldrich) for 1 h at room temperature. Then the beads were washed three times with IP buffer, boiled with SDS loading buffer, and used for immunoblotting.

Cell lysates for MAPK/NF-κB immunoblotting were prepared by lysing macrophages in SDS loading buffer followed by ultrasonication and protein quantification for loading of equal amounts.

For Western blot analyses, cell lysates or IP samples were separated on 4–12% Tris–Bis SDS/PAGE gels (Invitrogen) and blotted onto PVDF membrane (Millipore). Antibodies against FLAG, HA (both HRP-conjugated; Sigma Aldrich), V5 (HRP-conjugated; Invitrogen), phospho-p105, IκBα, phospho-p38, phospho-p42/44 (phospho-ERK), phospho-SAPK/JNK, total p38 (all Cell Signaling Technologies), and β-actin (HRP conjugated; Abcam) were used for detection.

Immunofluorescence. Bone marrow-derived macrophages from homozygous *cpdm* and littermate control mice were plated at 2.5×10^4 cells/well in glass-bottom, tissue-culture-treated 96-well plates (Cyntellect), allowed to adhere overnight, and then stimulated with 300 ng/mL Pam_3CSK_4. At specific times following stimulation, the media were removed, and the cells washed three times with PBS and fixed with 3% paraformaldehyde in PBS for 20 min at room temperature. All subsequent incubations were performed using antibody diluent (PBS with 0.1 mg/mL saponin and 0.5 mg/mL goat IgG), and all washes used PBS. Fixed cells were incubated for 45 min at room temperature in antibody diluent with 0.2 M glycine to block nonspecific antibody binding and to quench background fluorescence due to aldehydes. Cells were incubated for 60 min at room temperature with an anti–NF-κBp65 antibody (C-20; Santa Cruz; 200 μg/mL), diluted 1:50 in antibody diluent and Hoechst 33342 (200 ng/mL) (Invitrogen). Cells were incubated for 60 min with AlexaFluor-488 labeled goat anti-rabbit (2 mg/mL) diluted 1:200 in antibody diluent and washed four times for 10 min with PBS.

Fixed cells were imaged on a Delta Vision microscope (Applied Precision) with a 20× objective (NA = 0.75) at 0.32 μm/pixel in both the Hoechst (Ex. 360/40, Em. 457/50) and Alexa488 (Ex. 480/20, Em. 528/38) channels. Image analysis was performed with custom scripts written in MATLAB (MathWorks) (13, 14). The Hoechst and Alexa488 channels were segmented independently to identify the boundaries of nuclei and cells, respectively. The background level was determined by subtracting the median intensity in a region devoid of cells, and the average background-corrected intensity in the Alexa488 image within the nuclear and cell boundaries was computed. The extent of nuclear localization of p65 was inferred from the ratio of nuclear-to-cytoplasmic intensity ($p65^{Nuc.}/p65^{Cyto.}$). Differential localization between conditions was assessed by Wilcoxon rank-sum tests comparing ($p65^{Nuc.}/p65^{Cyto.}$) values for the largest subset of quantified cells in both conditions that were similar in terms of cell size, nucleus size, and overall brightness.

1. Gentleman RC, et al. (2004) Bioconductor: Open software development for computational biology and bioinformatics. *Genome Biol* 5:R80.
2. Dai M, et al. (2005) Evolving gene/transcript definitions significantly alter the interpretation of GeneChip data. *Nucleic Acids Res* 33:e175.
3. Irizarry RA, et al. (2003) Exploration, normalization, and summaries of high density oligonucleotide array probe level data. *Biostatistics* 4:249–264.
4. Vadigepalli R, Chakravarthula P, Zak DE, Schwaber JS, Gonye GE (2003) PAINT: A promoter analysis and interaction network generation tool for gene regulatory network identification. *OMICS* 7:235–252.
5. Wingender E (2008) The TRANSFAC project as an example of framework technology that supports the analysis of genomic regulation. *Brief Bioinform* 9:326–332.
6. Kielbasa SM, Gonze D, Herzel H (2005) Measuring similarities between transcription factor binding sites. *BMC Bioinformatics* 6:237.
7. Subramanian A, et al. (2005) Gene set enrichment analysis: A knowledge-based approach for interpreting genome-wide expression profiles. *Proc Natl Acad Sci USA* 102:15545–15550.
8. Benjamini Y, Hochberg Y (1995) Controlling the false discovery rate: A practical and powerful approach to multiple testing. *J R Statist Soc B* 57:289–300.
9. Eisen MB, Spellman PT, Brown PO, Botstein D (1998) Cluster analysis and display of genome-wide expression patterns. *Proc Natl Acad Sci USA* 95:14863–14868.
10. Lynn DJ, et al. (2008) InnateDB: Facilitating systems-level analyses of the mammalian innate immune response. *Mol Syst Biol* 4:218.
11. Smoot ME, Ono K, Ruscheinski J, Wang PL, Ideker T (2011) Cytoscape 2.8: New features for data integration and network visualization. *Bioinformatics* 27:431–432.
12. Schmitz F, et al. (2008) Mammalian target of rapamycin (mTOR) orchestrates the defense program of innate immune cells. *Eur J Immunol* 38:2981–2992.
13. Niemistö A, et al. (2007) Computational methods for estimation of cell cycle phase distributions of yeast cells. *EURASIP J Bioinform Syst Biol* 2007:46150.
14. Niemistö A, et al. (2006) Extraction of the number of peroxisomes in yeast cells by automated image analysis. *Conf Proc IEEE Eng Med Biol Soc* 1:2353–2356.

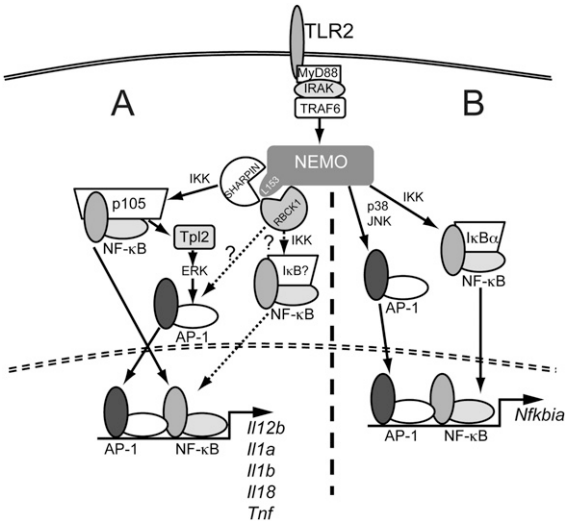

Fig. S1. SHARPIN is an essential adaptor downstream of the branch point defined by the *panr2* mutation in NEMO. (*A*) The signaling responses most strongly impaired by SHARPIN deficiency and NEMO L153P (*panr2*) are the phosphorylation of p105 and ERK, suggesting that p105 IκB activity and TPL2 sequestration are dominant regulators of Toll-like receptor 2 (TLR2)-induced proinflammatory cytokine expression. The greater deficiency in signaling and proinflammatory cytokine induction observed in *panr2* compared with *cpdm* macrophages may result from SHARPIN-independent interactions between NEMO and the SHARPIN paralog and the linear ubiquitin chain assembly complex constitutent RBCK1, which we found are also abrogated by NEMO L153P. (*B*) TLR2-induced IκBα degradation, phosphorylation of p38 and JNK, and *Nfkbia* gene induction were unimpaired in *cpdm* macrophages and *panr2* mutant macrophages, implying the existence of a branch of NEMO-dependent I-kappa-B kinase (IKK) and MAPK activity that proceeds independently of SHARPIN and NEMO residue L153.

Other Supporting Information Files

Dataset S1 (XLSX)
Dataset S2 (XLSX)